

Tetrahedra system  $\text{Cu}_4\text{OCl}_6\text{daca}_4$ : magnetic exchange against molecular vibrations

O. Zaharko,<sup>1</sup> J. Mesot,<sup>1</sup> L. A. Salguero,<sup>2</sup> R. Valent,<sup>2</sup> M. Zbiri,<sup>3</sup> M. Johnson,<sup>3</sup>  
Y. Filinchuk,<sup>4</sup> B. Klemke,<sup>5</sup> K. Kiefer,<sup>5</sup> M. Mys'kiv,<sup>6</sup> T. Strassle,<sup>1</sup> and H. Mütka<sup>3</sup>

<sup>1</sup>Laboratory for Neutron Scattering, ETHZ & PSI, CH-5232 Villigen, Switzerland

<sup>2</sup>Institut für Theoretische Physik, Universität Frankfurt, D-60438 Frankfurt, Germany

<sup>3</sup>Institut Laue-Langevin, 156X, F-38042 Grenoble Cedex, France

<sup>4</sup>Swiss-Norwegian Beam Lines, ESRF, F-38042 Grenoble, France

<sup>5</sup>BENSC, Hahn-Meitner Institut, D-14109 Berlin, Germany

<sup>6</sup>Institute for Inorganic Chemistry, Lviv State University, Lviv, Ukraine

(Dated: December 11, 2019)

The  $\text{Cu}_4\text{OCl}_6\text{daca}_4$  system composed of isolated  $\text{Cu}^{2+}$   $S=1/2$  tetrahedra with antiferromagnetic exchange should exhibit properties of a frustrated quantum spin system. Yet, extensive characterization of  $\text{Cu}_4\text{OCl}_6\text{daca}_4$  by means of synchrotron x-ray diffraction, magnetization, specific heat and inelastic neutron scattering reveals a complex interplay between magnetic exchange, molecular vibrations and plasticity of the  $\text{Cu}^{2+}$  coordination sphere while cooling. The experimental findings are reinforced by *ab initio* density functional theory calculations for electronic structure and molecular dynamics computations.

PACS numbers: 75.50.Xx, 36.40.Cg, 63.22.-m

## I. INTRODUCTION

Strongly frustrated quantum spin systems show, following numerous theoretical works<sup>1,2,3,4,5</sup>, highly degenerate ground states. When the degeneracy is lifted a number of exotic ground states may emerge. However, in spite of large experimental efforts such examples are rare and are hard to probe. Any perturbation tends to push the real system into a conventional classical ground state. A good recent example is the  $\text{Cu}_2\text{Te}_2\text{O}_5\text{X}_2$  ( $\text{X}=\text{Cl}, \text{Br}$ ) system. Being assumed to be built of weakly coupled tetrahedral units<sup>6,7,8,9,10,11</sup>, it appeared to have an incommensurate 3D long-range ordered ground state<sup>12</sup>. Our aim is to investigate the properties of tetrahedra which are the building blocks of geometrically frustrated quantum spin lattices (e.g. kagome, pyrochlore). Note that the ground state of an isolated tetrahedron with antiferromagnetic Heisenberg exchange is doubly degenerate in the case of high  $T_d$  symmetry. It is formed by two entangled<sup>11,14</sup> singlets; one being a product of two dimers  $\chi_1 = \frac{1}{4}(|\uparrow\uparrow\downarrow\downarrow\rangle + |\uparrow\downarrow\uparrow\downarrow\rangle - |\uparrow\downarrow\downarrow\uparrow\rangle - |\downarrow\uparrow\uparrow\downarrow\rangle)$  and the second composed by two-site triplet products,  $\chi_2 = \frac{1}{12}(2|\uparrow\uparrow\downarrow\downarrow\rangle + 2|\uparrow\downarrow\uparrow\downarrow\rangle - |\uparrow\downarrow\downarrow\uparrow\rangle - |\downarrow\uparrow\uparrow\downarrow\rangle - |\downarrow\uparrow\downarrow\uparrow\rangle - |\downarrow\downarrow\uparrow\uparrow\rangle)$ . Three triplets and one quintet constitute the excited states. We choose in the present work a simple frustrated quantum spin candidate among zero-dimensional systems.

We focus our study on the  $\text{Cu}_4\text{OCl}_6\text{L}_4$  system. Its main magnetic building block is an almost ideal isolated tetrahedral cluster of four  $\text{Cu}^{2+}$  ions (see Fig. 1). The magnetic properties of several representatives of this family could not be quantitatively accounted for by a simple Heisenberg isotropic exchange<sup>15,16,17</sup>. A number of more complex models have been proposed. In early stages Lines<sup>15</sup> suggested the existence of orbital degeneracy of the  $\text{Cu}^{2+}$  ion and a large antisymmetric contribution to

the spin Hamiltonian. However, angular overlap model calculations<sup>18</sup> indicated that the unpaired electron of the  $\text{Cu}^{2+}$  ion occupies the  $d_{z^2}$  nondegenerate orbital, which is ca. 960 meV above other d-orbitals. Henceforth the invoked models follow two routes, the first one exploits the complexity of the spin exchange and the second one puts forward the spin-vibrational interactions. The first approach is based on the generalized spin Hamiltonian

$$H_{\text{ex}} = H_{\text{iso}} + H_{\text{as}} + H_{\text{an}} = \sum_{ij} J_{ij} S_i S_j + \sum_{ij} G_{ij} (S_i - S_j) + \sum_{ij} \sum_{\alpha\beta\gamma\delta} X_{ij}^{\alpha\beta\gamma\delta} J_{ij} S_i S_j \quad (1)$$

where  $H_{\text{iso}}$  is the isotropic Heisenberg-Dirac-van Vleck term, and  $H_{\text{as}}$  and  $H_{\text{an}}$  are the antisymmetric and anisotropic terms respectively. A number of authors<sup>17,19,20</sup> explained magnetic susceptibility, electron paramagnetic resonance (EPR) and inelastic neutron scattering (INS) observations by considering large antisymmetric contributions (up to 20% of the isotropic exchange constant). Dickinson<sup>21</sup> suggested the presence of ferromagnetic intercluster exchange in addition to the antiferromagnetic intracluster one.

The second approach is based on the spin-vibrational Hamiltonian

$$H = H_{\text{vib}}(q) + H_{\text{ex}}(S; q) \quad (2)$$

where  $H_{\text{vib}}(q)$  describes the harmonic vibration of the nuclei around the equilibrium position and  $H_{\text{ex}}(S; q)$  depends not only on the spin  $S$  but also on the nuclear displacements  $q$  of the  $\text{Cu}^{2+}$  ions. Jones<sup>16</sup> developed a simplified model of dynamic and fluxional Jahn-Teller distortions of  $\text{Cu}_4\text{OCl}_6\text{L}_4$ , assuming a linear relation between the coupling constants and atomic shifts. Polinger<sup>22,23</sup> extended this approach concluding that the

pseudo Jahn-Teller effect is the most probable reason for the anomalous magnetic properties of the system. We collected substantial experimental data on  $\text{Cu}_4\text{OC}_6\text{L}_4$  with  $\text{L} = \text{diallylcyanamide} = \text{N}(\text{C}=\text{N}(\text{CH}_2-\text{CH}=\text{CH}_2)_2)$  ( $\text{Cu}_4\text{OC}_6\text{daca}_4$ ) and performed ab initio density functional theory calculations for electronic structure as well as ab initio molecular dynamics. Our findings suggest that indeed the vibrational degrees of freedom are very important. Nevertheless both, the generalized spin and spin-vibrational Hamiltonians remain insufficient to explain the measured magnetic properties of  $\text{Cu}_4\text{OC}_6\text{L}_4$ .

## II. EXPERIMENTAL DETAILS

The  $\text{Cu}_4\text{OC}_6\text{daca}_4$  single crystals (Nr. 1 and Nr. 2) and the polycrystalline sample have been prepared by reaction between  $\text{CuCl}$  and diallylcyanamide in the presence of  $\text{I}_2$ <sup>24</sup>. The crystal structure has been examined by X-ray synchrotron powder and single crystal diffraction performed at SNBL of ESRF at a wavelength of 0.7272 Å in the 80 K – 340 K temperature range.

The bulk properties have been studied using a Quantum Design PPM S commercial system. The dc- and ac-magnetic susceptibility of polycrystalline and single crystal materials have been measured in the 1.8 K – 300 K temperature range and in applied magnetic fields up to 9 T. The specific heat has been collected in 0.35 K – 10 K temperature range and in applied magnetic fields up to 14.5 T, and the magnetization – in the 1.8 K – 20 K temperature range up to 14.5 T.

The inelastic neutron scattering experiments have been performed on a 2 g polycrystalline protonated  $\text{Cu}_4\text{OC}_6\text{daca}_4$  sample on the neutron time-of-flight spectrometer FOCUS at SINQ and on a 0.5 g polycrystalline deuterated sample on IN4 at ILL. Four setups of FOCUS have been exploited ( $\lambda_i = 5.45$  Å, 4.87 Å, 3.42 Å and 2.26 Å) to access the 0 – 13 meV energy-transfer range with various energy resolutions. On IN4 high-energy transfers up to 40 meV have been probed with  $\lambda_i = 1.32$  Å, while a setup with  $\lambda_i = 2.64$  Å has been used for comparison with the FOCUS results on the protonated sample. Empty sample holders have always been measured and subtracted.

## III. CALCULATION METHOD

### A. Electronic structure

In order to understand the electronic and magnetic properties in this compound, first principles local spin density approximation calculations were done within the framework of the Density Functional Theory (DFT). For

the description of the exchange and correlation energy, the Generalized Gradient Approximation (GGA) was formulated by the Perdew-Burke-Ernzerhof (PBE) density functional<sup>25</sup>.

In the spin-polarized version of the GGA approximation the exchange-correlation energy  $E_{xc}$  is a functional of the local electron spin densities  $n_\uparrow$  and  $n_\downarrow$  and their gradients

$$E_{xc}^{GGA}[n_\uparrow; n_\downarrow] = \int d^3r f(n_\uparrow; n_\downarrow; r n_\uparrow; r n_\downarrow): \quad (3)$$

For calculating the eigenvalues and eigenvectors in the DFT scheme the Full Potential Linearized Augmented Plane Waves method (FP-LAPW), as implemented in the Wien2k code<sup>26</sup>, has been used. In this method the unit cell is divided in two regions, the first one is composed by non-overlapping spheres centered at the atomic sites and the second is the region between the atomic spheres or interstitial region. In the first region a spherical potential is assumed and therefore the wave functions are expanded in terms of spherical harmonics. In the interstitial region a constant potential is assumed. This allows to expand the wave functions in that region in terms of plane waves.

In our calculation the valence wave functions have been expanded up to  $l = 10$ . Sphere radii  $R_{mt}$  of 2.1 a.u. for the Cu atom, and 1.6, 1.4, 1.2, 0.9 and 0.84 u.a. for Cl, O, N, C and H atoms respectively have been set. Within the Cu muffin-tin chosen we excluded the 4s states (the average radii for the wave functions belonging to these states is 2.7 u.a.), therefore these states lie in the interstitial region. The Cu-3d and 3p states enter in the calculation as the valence and semicore states respectively, while for the Cu 3d states the LAPW basis with APW+lo have been used. The plane-wave expansion with  $R_{MT}K_{MAX}$  equal to 3.76 has been set. This is a typical value when C-H bonds are present. For the integration in the irreducible wedge, 48 k-points have been calculated.

### B. Molecular dynamics

The dynamics of Cu-daca have been investigated using the DFT code VASP<sup>27,28</sup> which is well adapted to a system as large as  $\text{Cu}_4\text{OC}_6\text{daca}_4$  (174 atoms per unit cell). VASP uses a plane wave basis set and PAW pseudo-potentials to describe the core electrons of the atoms. The GGA-PBE functional was used<sup>25</sup> and all electronic calculations were performed at the  $\Gamma$  point in reciprocal space. Since phonons and molecular vibrations are of interest in this paper, lattice dynamics calculations, involving the determination of the dynamical matrix, were attempted. In view of the number of atoms in the unit cell, the direct method<sup>29</sup> is the only practically feasible approach in which symmetry-inequivalent atoms are displaced one by one from equilibrium and the Hessian is constructed from the Hellmann-Feynman forces from the series of electronic calculations.

In the case of  $\text{Cu}_4\text{OC}_6\text{daca}_4$ , the direct method always resulted in negative frequencies. This method invokes a significant perturbation to the equilibrium conformation and therefore the electronic structure. Indeed, electronic and structural correlations between the core and the ligands lead to an electronic structure which is very sensitive to the precise molecular conformation. Such sensitivity is an indication of the fragility of this molecular system as proved by the physical meaning of negative frequencies in this case.

In this situation we resorted to *ab initio* molecular dynamics, using VASP, in which case the (partial) vibrational density of states ( $\rho$ )VDOS can be obtained from the velocity auto-correlation function and the scattering function is obtained from the van Hove correlation functions. Both of these correlation functions are determined directly from the *ab initio* molecular dynamics (AIMD) trajectories using the nMoldyn program<sup>30</sup>. The temperature dependence of the dynamics, which may reveal anharmonicity, is investigated via the average kinetic energy of the atoms. The drawback of the MD approach compared to a lattice dynamics calculation, is that the phase relation of the atomic displacements is lost and normal modes and their frequencies cannot be determined. One solution is to investigate the time-dependent fluctuations of geometric quantities associated with groups of atoms. In the case of the magnetic properties of  $\text{Cu}_4\text{OC}_6\text{daca}_4$  the Cu tetrahedron is of interest.

AIMD simulations have therefore been performed at 100 K and 250 K for a protonated crystal. Production simulations at constant volume and energy (NVE ensemble) cover 10 ps, that is  $10^4$  simulation steps. The 100 K simulation was then re-equilibrated for a deuterated crystal and the NVE production run in this case lasted 27 ps in order to give better access to the low frequency modes.

## IV. RESULTS

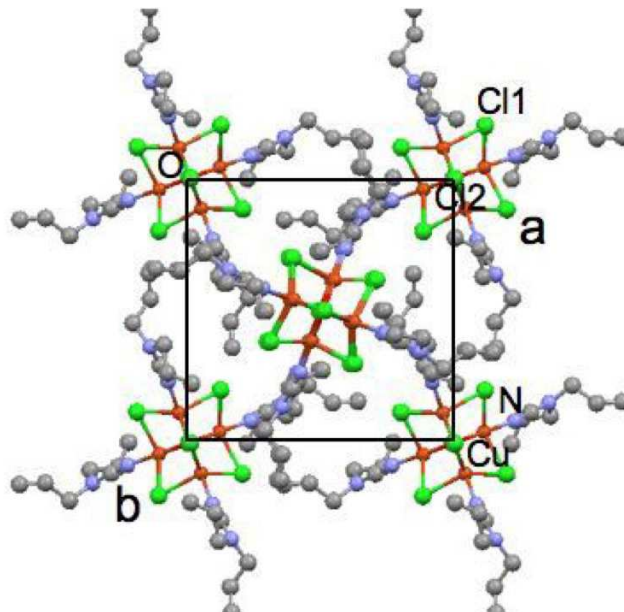
### A. Crystal structure

The  $\text{Cu}_4\text{OC}_6\text{daca}_4$  structure is tetragonal<sup>24</sup> (space group  $P\bar{4}2_1c$ ) in the whole 80 K – 340 K studied temperature interval. There are two  $\text{Cu}_4\text{OC}_6\text{daca}_4$  molecules per unit cell and they are slightly twisted around the  $z$  axis (Fig. 1). The oxygen is in the center of the molecule, surrounded by a tetrahedron of  $\text{Cu}^{2+}$  ions with two different Cu-Cu distances, equal to 3.0790 (2) Å and 3.1185 (2) Å at 80 K. The tetrahedron is enclosed by a distorted octahedron of chlorine ions with four  $\text{Cl}_1$  in the square base and two  $\text{Cl}_2$  in the apexes. Each copper has trigonal bipyramidal coordination: three  $\text{Cl}_1$  ions form the triangular base of the bipyramid, while the central  $\text{O}^{2-}$  ion and a terminal ligand L are located in apical positions. The exchange paths Cu-O-Cu are identical, while the two paths through chlorine ions, Cu- $\text{Cl}_1$ -Cu and Cu- $\text{Cl}_2$ -Cu,

slightly differ (see Table I). Such geometry implies rather high symmetry of the cluster and of the spin exchange Hamiltonian, only marginally deviating from  $T_d$ .

There is an anomaly in the lattice constants in the 230

FIG. 1: (Color online) The *ab* projection of the  $\text{Cu}_4\text{OC}_6\text{daca}_4$  unit cell. The Cu atoms are represented by orange circles,  $\text{Cl}_1$ , N and C – by green, red, blue and grey circles, respectively. H atoms are omitted for clarity, O are located behind  $\text{Cl}_2$  and, therefore, are not visible.



K – 280 K temperature range notifying an isostructural order-disorder crossover<sup>31</sup>. Apparently the molecule attains several conformations with small energy difference between them. Above  $T_c = 282$  K these conformations coexist, while below  $T_c$  molecules freeze in one of them. The conformations differ mainly by the position of the branched dialkylcyanamide ligands, which fold. This modifies the distances between the molecules (Table I) and the unit cell volume shrinks by 7% at 80 K compared to the volume at room temperature. The  $\text{Cu}_4\text{OC}_6\text{N}_4$  core changes very little. The only noticeable difference is the shift of the  $\text{Cl}_1$  ions by 0.2487 (9) Å, while for Cu and  $\text{Cl}_2$  the shift is only 0.0462 (9) Å and 0.0282 (9) Å, respectively.

Inspection of the interatomic distances and angles presented in Table I suggests that the Cu-O-Cu magnetic exchange path is antiferromagnetic (AF), while the Cu- $\text{Cl}_1$ -Cu one is ferromagnetic (F). Therefore the mobility of the  $\text{Cl}_1$  ions is essential in determining the magnetic exchange.

One more appreciable detail could be extracted from the single crystal diffraction data. The difference Fourier map through the N-O-N plane of the molecule (Fig. 2) shows additional electron density near Cu atoms at 80 K. The tiny peaks (0.38 and 0.31 e/Å<sup>3</sup>) are displaced along  $z$  by 0.84 (5) Å and 0.73 (10) Å from Cu towards O

and N (Figure 2), respectively. At 300 K these peaks are less pronounced ( $0.24 e/A^3$ ). These difference electron density peaks near Cu and O, N, C positions evidence the delocalization of  $e$ -density in the O-Cu-N C bonds. No smearing of electron density near copper atoms or an increase of their anisotropic displacement parameters is observed implying the absence of a static and/or dynamic Jahn-Teller effect at 80 K. It should be noted that mean-square displacement amplitudes at 80 K are very small (see Table I).

FIG. 2: Difference Fourier map of  $Cu_4OCl_6daca_4$  at 80 K (top) and 300 K (bottom) from x-ray single crystal data.

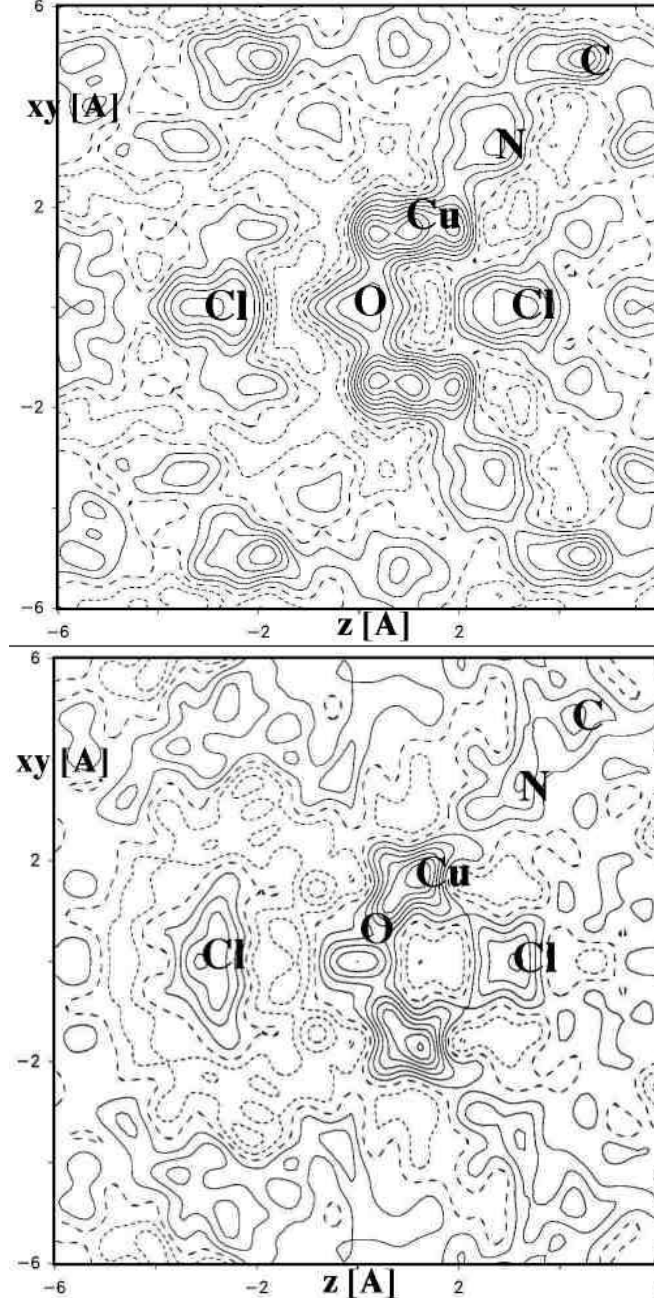


TABLE I: Characteristic intracenter distances ( $d_{intra}$  [Å]) and angles [deg] in  $Cu_4OCl_6daca_4$  at 80 K. Comparison of the distances between the centers of the molecules in the unit cell ( $d_{inter}$ ) at 80 K and 300 K. Mean-square displacement amplitudes of Cu ( $MSD_{Cu}$  [Å<sup>2</sup>]) and other atoms ( $MSD_{lig}$ ) in the specified bond directions of the  $CuCl_3ON$  trigonal bipyramid calculated from the anisotropic displacement parameters refined at 80 K.

$d_{intra}$	80 K	300 K	Angles	80 K	300 K
Cu-Cu	3.0790 (2)	3.0933 (4)	$\backslash_{CuOCu}$	108.106 (6)	108.9 (2)
Cu-Cu	3.1185 (2)	3.1101 (5)	$\backslash_{CuOCu}$	110.158 (6)	109.8 (2)
Cu-O	1.9017 (1)	1.9011 (3)	$\backslash_{NCuO}$	179.01 (4)	178.8 (1)
Cu-N1	1.933 (1)	1.935 (3)	$\backslash_{CuClCu}$	80.46 (1)	80.48 (3)
Cu-C11	2.3696 (3)	2.3912 (9)	$\backslash_{CuClCu}$	80.59 (1)	80.62 (3)
Cu-C12	2.3804 (3)	2.3909 (8)	$\backslash_{CuClCu}$	117.97 (1)	118.84 (3)
Cu-C11	2.4574 (3)	2.4321 (9)	$\backslash_{CuClCu}$	111.849 (9)	117.98 (3)
	$MSD_{Cu}$	$MSD_{lig}$	$d_{inter}$	80 K	300 K
Cu-O	0.0107	0.0125	$d_{100}$	12.60490 (3)	12.5652 (1)
Cu-C11	0.0143	0.0130	$d_{001}$	12.73045 (5)	13.7685 (2)
Cu-C12	0.0203	0.0189	$d_{111}$	10.9525 (3)	11.2399 (1)
Cu-N1	0.0108	0.0152			

#### B. Electronic structure and charge density distribution

The electronic Density of States (DOS) has been calculated for the crystal structures determined at temperatures, 80 K and 340 K. Since both structures have almost indistinguishable DOS features, we present here the results for the  $T = 80$  K structure. In Figure 3 we show the partial Cu  $d$ , Cl  $p$ , N  $p$ , O  $p$  and C  $p$  DOS in the range of energies between -4 and 4 eV obtained from non-spin polarized GGA<sup>25</sup> calculations. We observe a very narrow and sharp contribution of Cu  $d$  and Cl, N and O  $p$  states at the Fermi level well separated from the rest of the valence and conduction states. These features indicate that these states strongly hybridize and that the system is almost zero dimensional, formed by well isolated Cu tetrahedra. The bandwidth at the Fermi level is less than 0.2 eV (see the inset of Fig. 3 where a blow up of the DOS at the Fermi level is shown). From calculations of the crystal field splitting we conclude that the Cu  $d$  band at the Fermi level has  $d_{z^2}$  character (in the local reference frame of the  $CuCl_3ON$  trigonal bipyramid).

Within the GGA approximation<sup>25</sup> we obtain that the Cu  $d$  states are partially occupied and therefore the system is metallic. This is a well-known drawback of DFT calculations within the LDA or GGA approach when performed for correlated systems. Improved exchange-correlation functionals like LDA+U<sup>32</sup> should provide the correct insulating behavior of the material. In the case of Cu-daca, calculations at the level of spin-polarized GGA already open a small gap at the Fermi level as shown in Fig. 4. In this figure we present the partial DOS for Cu  $d$  states in both spin up (upper panel) and spin down (lower panel) channels. The occupation of the spin-up

and spin-down Cu d states is very similar, therefore the resulting localized magnetic moment is small. The Table II presents the magnetic moment at the cluster core inside the muffin-tin radii. The unpaired Cu electron is strongly delocalized via hybridization mainly with oxygen and less strongly with chlorine and nitrogen.

In Fig. 5 we show the projection on the xy plane of the calculated charge density map of the band around the Fermi level. We note the good agreement with the measured difference Fourier map from the 80 K x-ray diffraction experiment (Fig. 2).

FIG. 3: (Color online) Partial Density of States in the non-spin polarized GGA calculations for  $\text{Cu}_4\text{OCl}_6\text{daca}_4$  at  $T = 80$  K.

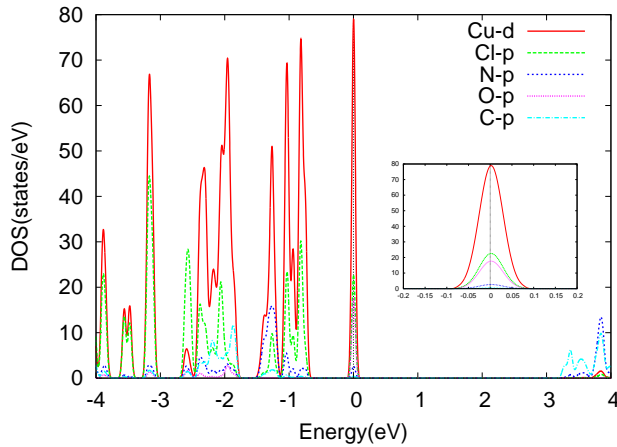


FIG. 4: Partial Density of States for majority (upper panel) and minority (lower panel) spin contributions from Cu-d states for  $\text{Cu}_4\text{OCl}_6\text{daca}_4$  at  $T = 80$  K.

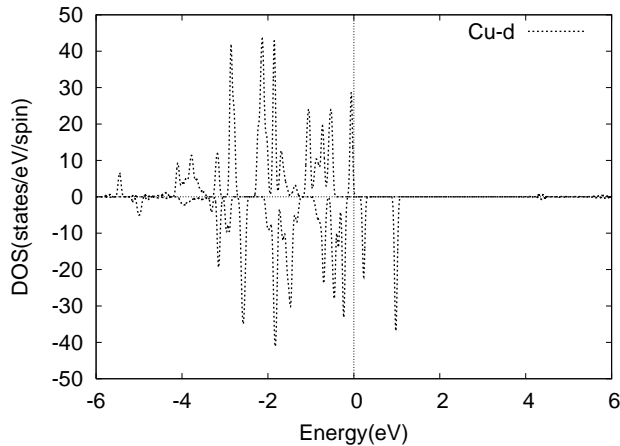


FIG. 5: (Color online) Charge density distribution at  $T = 80$  K.

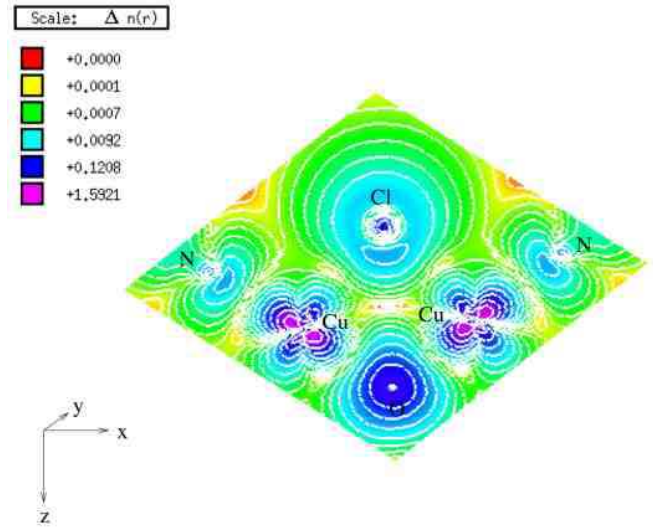


TABLE II: Magnetic moment ( $M$  [ $m_B$ /atom]) within the muffin-tin radii ( $r_{mt}$ ) and its total moment fraction [%]. For the interstitial the moment is normalized per formula unit ( $\text{Cu}_4\text{O}_{0.25}\text{Cl}_{1.5}\text{daca}_4$ ).

Atom	$r_{mt}$	$M$	
Cu	2.1	0.58350	58
O	1.4	0.44204	11
Cl I	1.6	0.08352	8.3
Cl 2	1.6	0.09027	4.5
N 1	1.2	0.02857	2.9
interstitial		0.14477	14

### C. Bulk properties

The temperature dependence of dc-magnetization ( $M/H$ ) measured for the polycrystalline sample at  $H = 0.1$  T and for a single crystal (N r. 1) at several values of applied magnetic field is presented in Fig. 6. At 300 K the ( $M/H$ )  $T$  value is  $0.375 \text{ cm}^3 (\text{mol Cu})^{-1} \text{ K}$  suggesting that the system is composed of uncoupled  $S = 1/2$  spins. The Curie-Weiss temperature estimated from the high-temperature susceptibility is  $\theta_1 = 50$  K, which implies dominant antiferromagnetic interactions.

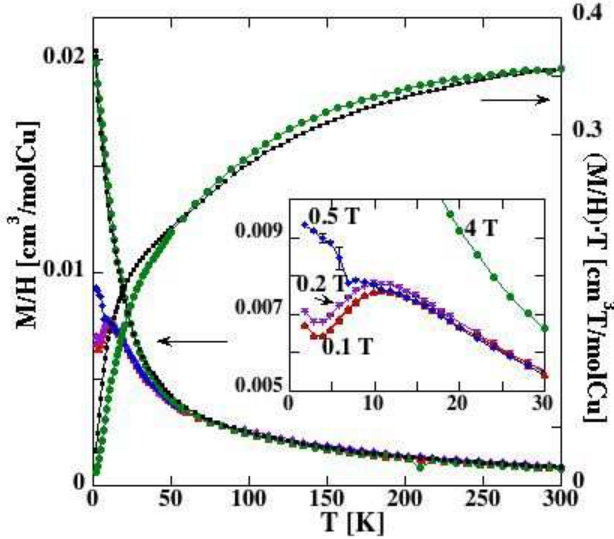
For the polycrystalline sample  $M/H$  gradually increases with temperature lowering and at 1.8 K reaches  $0.02 \text{ cm}^3 (\text{mol Cu})^{-1}$ . This is a very small value, suggesting the presence of tiny amount of free  $S = 1/2$  impurities. However, the temperature dependence cannot be fitted to a Curie-like  $1/T$  contribution, which would grow much faster at low temperatures.

For a single crystal dc-magnetization consists of two major contributions. The first contribution has a bump near 12 K and can be attributed to isolated tetrahedra with antiferromagnetic exchange resulting in a spin-

singlet ground state. The second contribution increases with temperature and, similarly to the polycrystalline case, cannot be fitted to the paramagnetic  $1/T$  term. The ratio of these contributions is different for different single crystals and depends on crystal orientation and applied magnetic field. Based on a number of dc-magnetization measurements we reckon that sensitivity to magnetic field is related not to a specific crystallographic direction but to the morphology of crystal; apparently there is a growth anisotropy and not a lattice anisotropy.

Crystals usually grow as platelets with the [110] axis di-

FIG. 6: (Color online) Temperature dependence of dc-magnetization ( $M/H$ ) of the single crystal Nr. 1 measured at 0.1 T, 0.2 T, 0.5 T, 4 T and of polycrystalline (black solid line)  $\text{Cu}_4\text{OCl}_6$  measured at 0.1 T (left scale). ( $M/H$ )  $T$  of crystal and powder measured at 0.1 T (right scale). Inset: zoomed 1.8 K – 30 K temperature interval of  $M/H$  of the crystal.

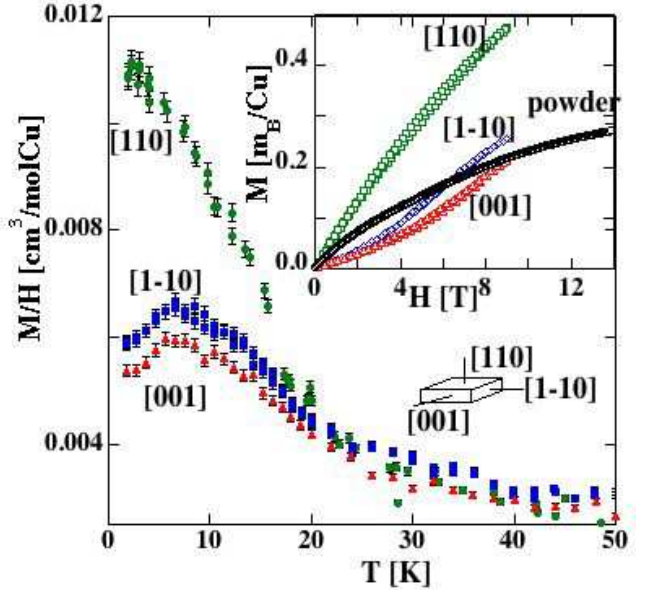


rected along the shortest edge, and [001] and [1-10] being in the most developed plane. An example of  $M/H$  extremely sensitive to the field is presented in inset of Fig. 6. The measurement is performed with magnetic field applied along the shortest edge. With increasing field the bump at low temperatures decreases and already at  $H = 0.5$  T vanishes.

For another crystal (Nr. 2)  $M/H$  shows no bump along the shortest edge even at  $H = 0.2$  T (Fig. 7), though when magnetic field is applied along the middle [001] or long [1-10] edges of the crystal, the bump is tractable to much higher fields (not shown). Interestingly, heating the crystal up to 120 K does not restore the initial state, while warming up to 300 K does.

The field dependence of dc-magnetization is also sample and direction dependent (Fig. 7 inset). For the polycrystalline sample magnetization is concave and does not saturate at 14 T reaching only  $0.27 m_B / \text{Cu}$ . For the single crystal 2 magnetization attains almost  $0.5 m_B / \text{Cu}$

FIG. 7: (Color online) Temperature dependence of dc-magnetization ( $M/H$ ) of the single crystal Nr. 2 measured with magnetic field  $H = 0.2$  T applied along three crystallographic directions: [110] (green circles), [001] (red triangles) and [1-10] (blue squares), corresponding to short, middle and long edges of the crystal. Inset: Field dependence of dc-magnetization of single crystal 2 and powder  $\text{Cu}_4\text{OCl}_6$  data at 1.8 K.



for the [110] direction, while for other directions it approaches values similar to the polycrystalline sample. The presented single crystal and polycrystalline bulk data cannot be modeled within the generalized spin Hamiltonian (eq. 1) even allowing unreasonably large anisotropy or asymmetry terms. The most plausible scenario explaining all our observations is a nonuniform distribution of intratetrahedral exchange couplings within a single crystal and – even to larger extent – within a polycrystalline sample. We reinforce such picture by a  $M/H$  calculation for a model comprising two types of clusters, (i) with isotropic AF exchange  $J = 20$  K, (ii) with three AF ( $J = 20$  K) and three F ( $J_{1j} = 20$  K<sup>33</sup>,  $j = 2 \dots 4$ ) couplings, and a small paramagnetic contribution. In such case the magnetic susceptibility ( $M/H$ ) can be written as

$$= \chi_1 + \chi_2 + \chi_3 \quad (4)$$

with

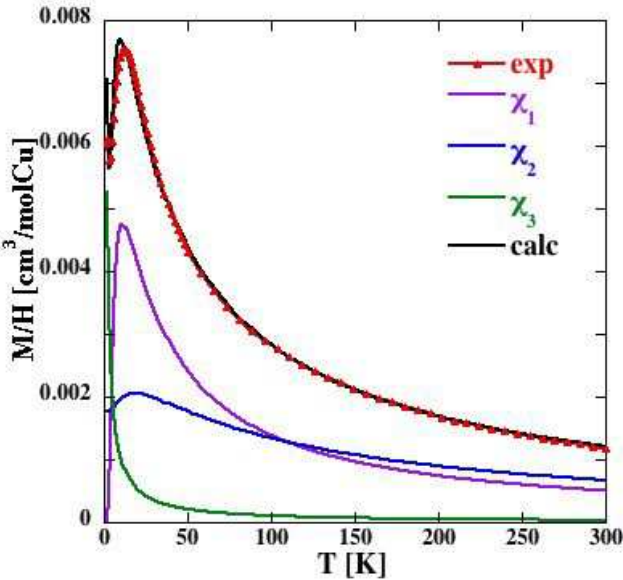
$$\chi_i = C_i \frac{S(S+1)(2S+1)e^{E_{is}=kT}}{S(2S+1)e^{E_{is}=kT}} \quad (5)$$

$\chi_1$  is the susceptibility of the isolated AF clusters ( $C_1 = \frac{N_1 \mu_B^2 g^2}{3kT}$ ),  $\chi_2$  is the susceptibility of the AF/F clusters coupled via an AF intercluster exchange ( $C_2 = \frac{N_2 \mu_B^2 g^2}{3k(T - T_2)}$ ).  $\chi_3 = c_3/T$  is the paramagnetic contribution. The best fit for  $M/H$  of the crystal 1 measured at  $H = 0.1$  T is

presented in Fig. 8. It corresponds to  $c_1 = 0.106(1)$ ,  $c_2 = 0.1772(9)$  and  $c_3 = \frac{2N_3 \mu_B^2 g^2}{3kT} = 0.0105(1)$  implying that the crystal Nr. 1 is composed of 1/3 of AF clusters and 2/3 of AF/F clusters. According to the fit, AF/F clusters are coupled by a short-range AF intercluster exchange with  $J_2 = 98(2)$  K. Neglecting this exchange or introducing intercluster exchange between AF clusters results in much worse fits. Surely such intercluster correlations is unrealistic for the ideal  $\text{Cu}_4\text{OC}_6\text{H}_6\text{daca}_4$  system, as the distances between molecules are too large (see Table I). Yet the presence of such interactions is feasible when numerous defects on grain boundaries are taken into account. These defects are formed, while cooling through  $T_C$  at the order/disorder phase transition<sup>34</sup> and are extremely dependent on sample growth and on thermal treatment. Therefore different single crystals have different  $c_1$ ,  $c_2$  and  $c_3$  contributions. In polycrystalline samples the concentration of defects is the largest, consequently the contribution of isolated AF clusters is overwhelmed by the two others.

The presence of defects leading to AF/F clusters and

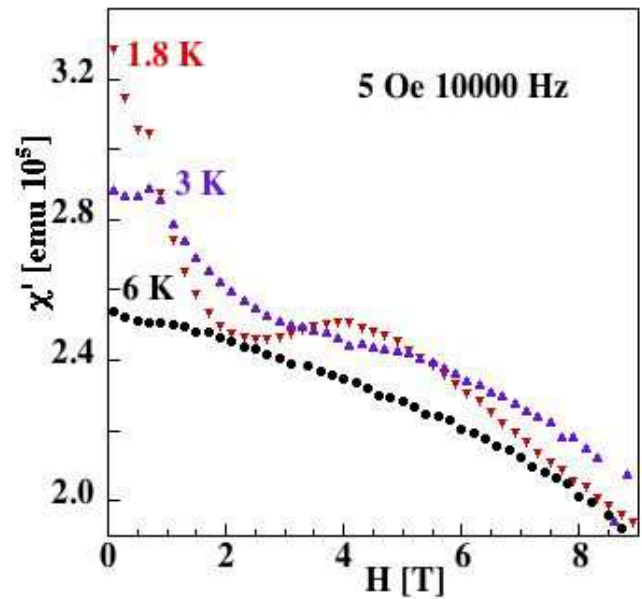
FIG. 8: (Color online) Calculated (black) and experimental (red) dc-magnetization ( $M/H$ ) of the single crystal Nr. 1, as well as the separate contributions of AF clusters  $\chi_1$  (violet), of AF/F clusters  $\chi_2$  (blue) and the paramagnetic term  $\chi_3$  (green).



intertetrahedral couplings between them causes the sensitivity of the bulk properties to the applied magnetic field which is significantly smaller than  $J$ . The real part of the ac-susceptibility of polycrystalline sample shows several steps as a function of applied field (Fig. 9). The most pronounced step is between 2 T – 4 T, which corresponds to the Zeeman energy of 0.24 m eV – 0.48 m eV. Also the low temperature specific heat of polycrystalline and single crystal samples contains a broad Schottky-type anomaly

centered at 0.4 K (0.034 m eV) in 0- field data (Fig. 10). This feature shifts to higher temperatures with applying field. The magnetic entropy extracted below 10 K after subtraction of a constant phonon contribution reaches only 0.7-0.8 J/K mol Cu. This is approximately 1/8 of the  $R \ln 2 = 5.763$  J/K mol Cu value expected for the spin degree of freedom, so this magnetic contribution corresponds to a minor part of the sample. We deduce that one of the triplet E-levels of AF/F clusters is situated at 0.4 K, though collected data are insufficient to propose the full energy scheme for AF/F clusters.

FIG. 9: (Color online) Real part of ac-susceptibility of polycrystalline  $\text{Cu}_4\text{OC}_6\text{H}_6\text{daca}_4$  measured in applied magnetic field up to 9 T at 1.8 K, 3 K and 6 K.

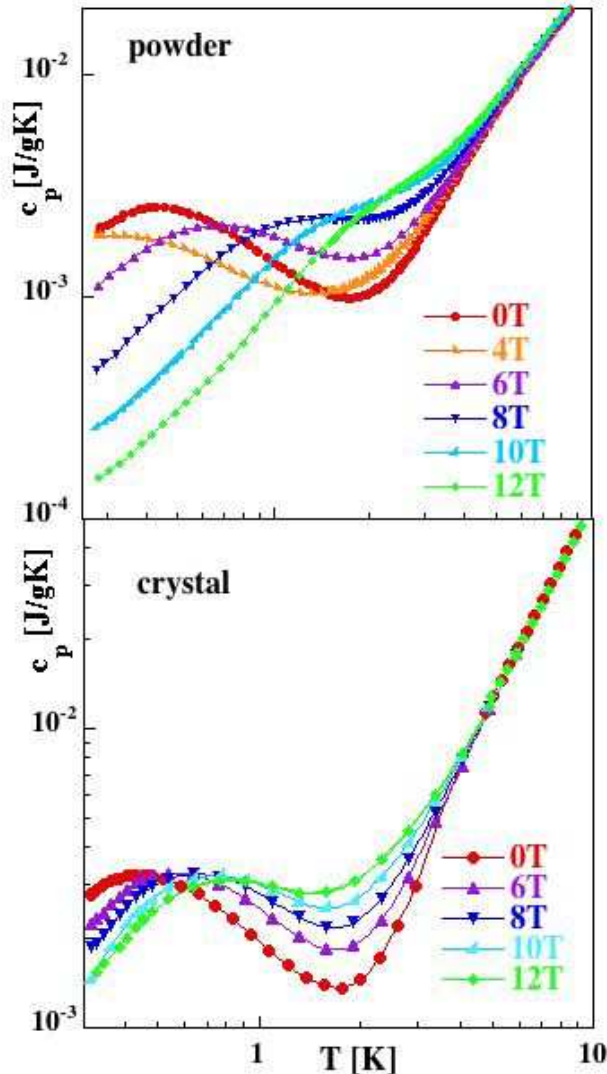


#### D. Inelastic neutron scattering

For the protonated sample at 2 K two sharp features have been detected at 1.8 m eV and 2.4 m eV on the neutron energy loss side, they are labeled 1 and 2 in Fig. 11. The peaks are at least two times broader than the resolution function (0.08 m eV at 1.8 m eV). At higher temperatures (7 K, 15 K, 35 K) the 1.8 m eV feature broadens and shifts to lower energies or a 2nd peak at slightly lower energy of 1.6 m eV appears and increases in intensity, while the 1.8 m eV peak decreases. The 2.5 m eV feature increases in intensity and an additional feature at 1 m eV (labeled 3) appears. No extra peaks have been observed in the low energy region down to 0.4 m eV.

A number of peaks are observed at higher energy transfers, of which the most pronounced is the one at 4.8 m eV, denoted 4 in Fig. 12. Its width is at least three times broader than the resolution function (0.3 m eV at

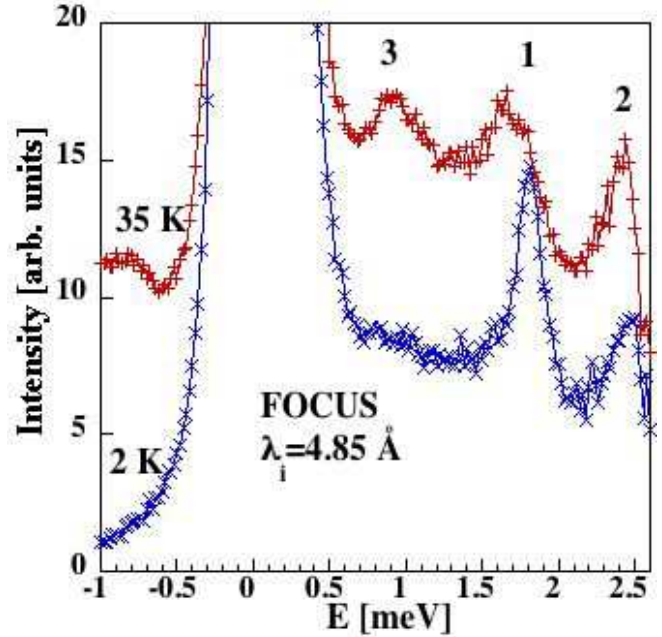
FIG. 10: (Color online) Log/log plot of specific heat of polycrystalline (top) and single crystal (bottom)  $\text{Cu}_4\text{OCl}_6\text{dca}_4$  in the 0.28 K – 10 K temperature range with applied magnetic field 0 T – 12 T.



4.8 meV) and intensity increases from 2 K to 35 K. The measurements on deuterated sample reveal essentially the same excitation spectrum (Fig. 13). The 1.8 meV peak tends to vanish at 75 K, while the 2.4 meV and 4.8 meV features decrease from 2 K to 75 K. From the  $Q$  (momentum)- and  $T$  (temperature)-dependence we relate the 1.8 meV peak to a spin singlet-triplet transition between the cluster levels, though it is not clear if it is a single excitation or several ones. The 4.8 meV feature is increasing with  $Q$  and most probably is related to molecular vibrations, while for the 2.4 meV and other features the FOCUS and IN4 results are less conclusive. The measurement at higher energy transfers showed that relatively sharp peaks discussed above reside on a very

broad feature (up to 20 meV), which increases in intensity with temperature and  $Q$  (Fig. 14). This feature is akin to vibration modes of the cluster as follows from the MD calculations presented below.

FIG. 11: (Color online) INS spectra of protonated  $\text{Cu}_4\text{OCl}_6\text{dca}_4$  at  $T=2$  K (blue) and 35 K (red) measured on FOCUS with  $\lambda_i=4.85$  Å. The intensity has been integrated over the momentum transfer range  $0.5 < Q < 2$  Å<sup>-1</sup>.



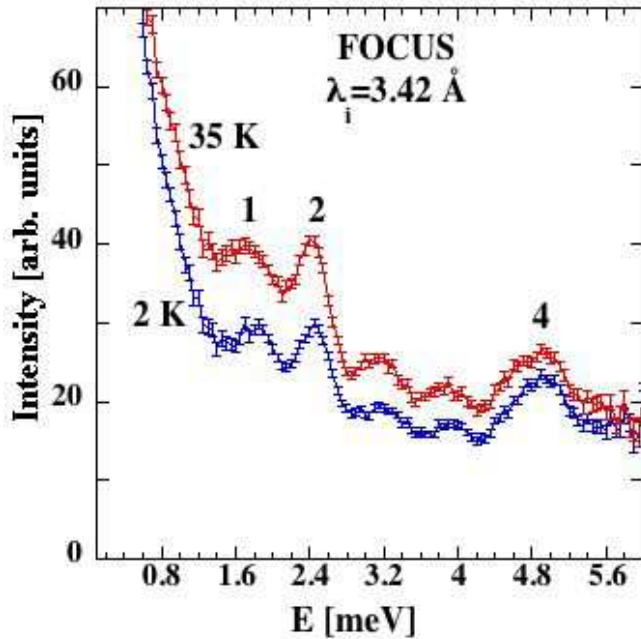
### E. Molecular dynamic

AIMD simulations give a direct view of the amplitude of atomic displacements. While the light atoms tend to have larger displacements than the heavier atoms (Cl and Cu), this is not the case for O which is trapped in the Cu-tetrahedron and the Cl-octahedron. Note that the atoms are classical particles in the AIMD simulations so that their displacements do not include zero-point motion, which can be of the order of 30% for hydrogen at room temperature. Calculated mean-square displacements (MSD) averaged over all atoms of the same type are 0.0177 Å<sup>2</sup> for Cu, 0.0300 Å<sup>2</sup> for Cl, 0.0093 Å<sup>2</sup> for O and 0.0283 Å<sup>2</sup> for N. This is in good agreement with values obtained by projection on specific bond directions from the 80 K crystal structure refinement listed in Table I.

The MD simulations are validated by comparing calculated and measured scattering functions (Figs. 11–14). We note that the low frequency modes are independent of H/D substitution and must therefore be delocalized modes involving many atoms. An acoustic phonon would show a 2% frequency shift upon deuteria-

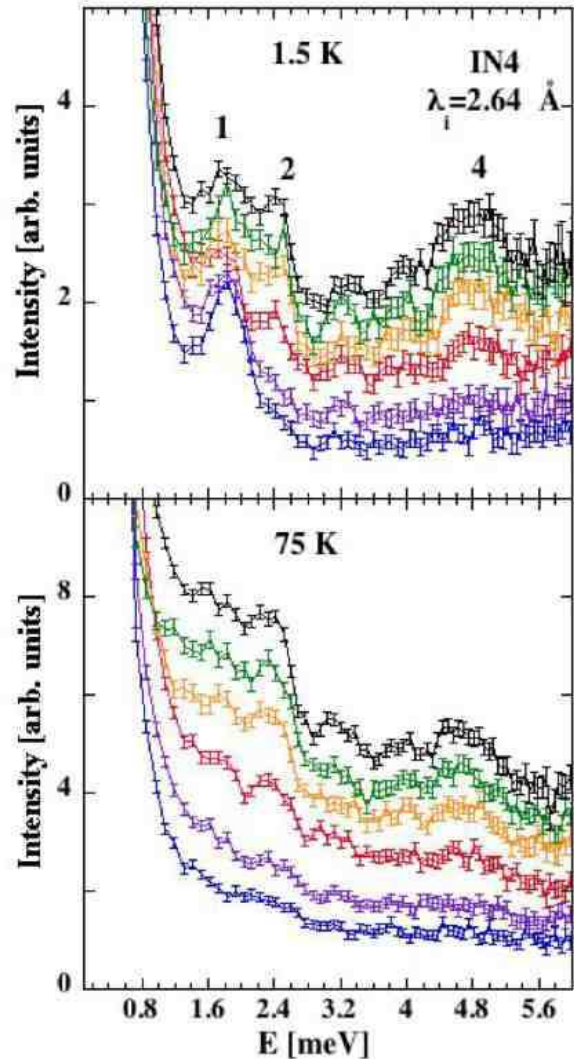


FIG. 12: (Color online) INS spectra of protonated  $\text{Cu}_4\text{OC}_6\text{daca}_4$  at  $T=2\text{ K}$  (blue) and  $35\text{ K}$  (red) measured on FOCUS with  $Q_i=3.42\text{ \AA}^{-1}$ . The intensity has been integrated over all available  $1 < Q < 2.6\text{ \AA}^{-1}$  range.



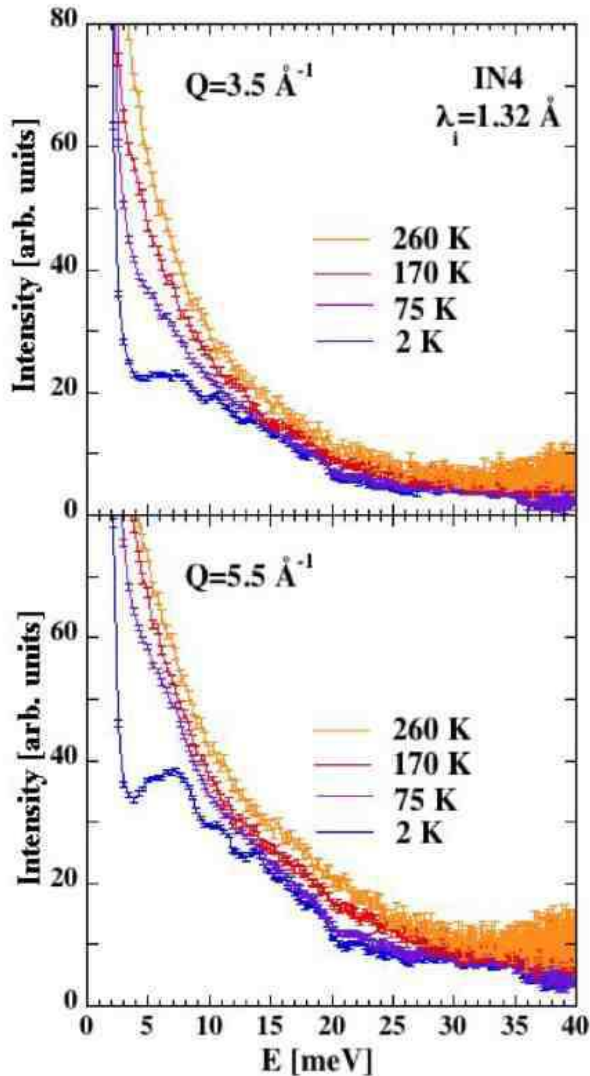
tion. Fig.15 shows  $S_{\text{coh}}(Q; \omega)$  from the 27 ps simulation on the deuterated system. Spectra at lower  $Q$ -values have weak intensity and are not reliably calculated with our model. Low frequency, numerical noise in the vDOS contributes strongly to the CSF since CSF is proportional to vDOS/frequency. At high  $Q$  there are peaks at 2 meV, 4.5 meV and 7 meV and a shoulder at 10 meV which are consistent with the experimental data. Since the AIMD simulations do not include spin degrees of freedom, these peaks can only be the signature of lattice excitations and, as expected, their intensities increase with increasing  $Q$ . The coherent scattering function is only calculated at the reciprocal lattice points of the simulation cell so that  $Q$ -sampling is limited to the Brillouin zone centres when using a single cell for the MD simulations. Simulated spectral peaks therefore correspond to Gamma point modes. Atomic contributions to the signal are best considered from the pVDOS which are shown in Fig.16. Each pVDOS has been normalized to the corresponding number of degrees of freedom,  $3n$ , where  $n$  is the number of a particular species. Fairly well-defined peaks exist at the lowest frequencies in the low temperature MD simulations. The delocalized nature of the modes is shown by the fact that all atoms have similar pVDOS's below 5 meV. This result is consistent with there being negligible spectral shift upon deuteration. The trapped oxygen atom has a characteristic vibration frequency of the order of 55 meV and this is the only atom that does not contribute to the lowest frequency modes. The analysis

FIG. 13: (Color online) INS spectra of deuterated  $\text{Cu}_4\text{OC}_6\text{daca}_4$  at  $T=2\text{ K}$  (top) and  $75\text{ K}$  (bottom) measured on IN4 with  $Q_i=2.64\text{ \AA}^{-1}$  for six  $Q$ -values ranging, with increasing intensity, from 1 to  $3.5\text{ \AA}^{-1}$  integrated over  $0.5\text{ \AA}^{-1}$ .



of the chlorine atoms has been refined to separate the contributions from apical atoms and those in the square base around the copper tetrahedron. There is a small but significant softening of the apical-chlorine vibrations compared to those of the square-base chlorines, average frequencies and standard deviations being, respectively, 18.8 13.5 meV and 20.3 14.4 meV. Fig.16 shows examples of the lowest frequency part of the VDOS for D, C and Cu for different lengths of simulations. The dotted curves show the results from a 10 ps trajectory while the solid curves are derived from the 27 ps trajectory. The longer trajectory gives better frequency resolution which shows that the first peaks in the DOS occur at 2 meV. Spectral peaks below this frequency must therefore be of

FIG. 14: (Color online) INS spectra of deuterated  $\text{Cu}_4\text{OCl}_6\text{daca}_4$  at  $T = 2\text{ K}, 75\text{ K}, 170\text{ K}$  and  $260\text{ K}$  measured on IN4 with  $Q_i = 1.32\text{ \AA}^{-1}$ . The intensity has been integrated over  $1\text{ \AA}^{-1}$ .



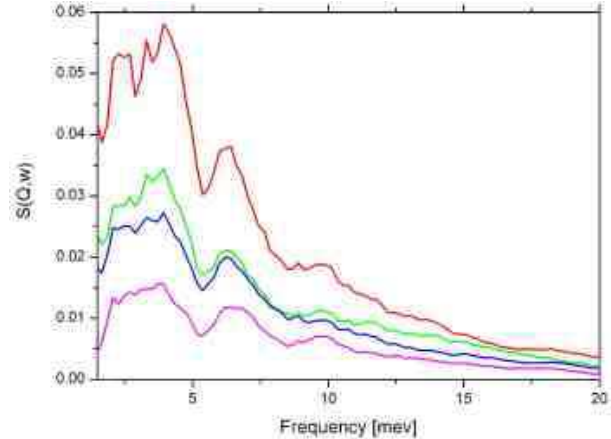
magnetic origin.

Features of the VDOS can be further understood by considering  $n$ -atom correlations. The frequency spectrum of interatomic distances involving Cu atoms is shown in Fig.17. The Cu-Cu stretch is strongest at  $12\text{ meV}$ . The twisting deformation of the tetrahedron, that is the angle variation between Cu-Cu vectors on opposite sides of the tetrahedron, also has a characteristic frequency of  $12\text{ meV}$ . These are the modes that could directly modulate the magnetic copper-copper interactions. The oxygen pathway is clearly not modulated by any low frequency modes whereas the copper-chlorine distance modulations show a significant amplitude from  $25\text{ meV}$  down to the lowest frequencies.

Spin restricted AIMD simulations are the only way to

gain insight into the low frequency modes of a sm measured on FOCUS and IN4. Simulations show excitations at above  $2\text{ meV}$  and at  $4.5\text{ meV}$  which grow in intensity with  $Q$  and therefore correspond mainly to molecular vibrations. Below these frequencies, the longest simulations ( $27\text{ ps}$ ) indicate that there are no lower lying lattice vibrations implying that the lower energy features observed in experiment are of the magnetic origin.

FIG. 15: (Color online) Calculated coherent scattering function (CSF) for four  $Q$ -values ranging, with increasing intensity, from  $2.5$  to  $5.5\text{ \AA}^{-1}$  of deuterated  $\text{Cu}_4\text{OCl}_6\text{daca}_4$ .



## V. SUMMARY

The  $\text{Cu}_4\text{OCl}_6\text{daca}_4$  system comprises very interesting magnetic unit – a  $\text{Cu}^{2+} S = 1/2$  tetrahedron. Due to the geometry of the cluster two exchange paths are possible: antiferromagnetic Cu-O-Cu via the central oxygen atom and ferromagnetic Cu-Cl-Cu via the peripheral chlorine atoms. In the ideal system the AF exchange with  $J = -1.8\text{ meV}$  dominates.

Our DFT calculations show that unpaired electron is only partially localized in the Cu d-states, and is transferred to the oxygen atom in the center of the tetrahedron and is further delocalized around atomic cores within the molecule. Besides the  $\text{O}^{2-}$  and  $\text{Cl}^-$  ions, which certainly participate in the Cu-Cu superexchange, the N-C bond might play an important role of the charge reservoir. We plan to confirm this picture by polarised neutrons spin density mapping and to study interplay between electron delocalization and magnetic interactions more in details.

The presence of strong molecular vibrations emerge from our INS experiments and spin restricted AIMD simulations. Albeit all atoms participate in the vibrations, it is the ligands and the apical Cl ions of the cluster which vibrate most strongly, while  $\text{O}^{2-}$  ion remains pinned in the center of the tetrahedron. Therefore the spin-vibrational Hamiltonian suggested by Jones<sup>16</sup> and Polinger<sup>22,23</sup> is the most appropriate model to describe

the ideal  $\text{Cu}_4\text{OCl}_4$  system.

However, the properties of real samples, cannot be that easily attributed to this model. Due to the isostructural order/disorder structural transition at  $T_c = 282$  K and to the high plasticity of the  $\text{Cu}^{2+}$  coordination sphere, the quality of crystals becomes worse during cooling. This modifies the exchange interactions weakening the AF Cu-O-Cu exchange in favor of the F Cu-Cl-Cu one. Measurements of the bulk properties reveal that only part of the clusters retain the spin singlet ground state, another part has magnetic ground state and the ratio between these fractions is sample- and growth direction-dependent. Moreover, apparently there exists an AF intertetrahedral exchange between the AF/F clusters and this exchange can be easily modified by applied magnetic field.

The complications of the real samples hinder answering the initial question which motivated our research, namely

whether the ground state of an isolated tetrahedron with antiferromagnetic exchange remains degenerate or this degeneracy is easily lifted by some small perturbation. Our study reveals that the behaviour of such "simple" systems is quite complex and is governed by an interplay of magnetic and vibrational degrees of freedom.

## VI. ACKNOWLEDGMENTS

Discussions with Drs. P. Tregenna-Piggott, D. Chernyshov, A. F. Albuquerque, Prof. S. K. Banishner are highly acknowledged. The work was partially performed at SINQ, Paul Scherrer Institute, Villigen, Switzerland. We thank for access to a Quantum Design magnetometer of University of Bern.

\* e-mail: Oksana.Zaharko@psi.ch

- 1 C. W. Akhtamann, H.-U. Everts, B. Bernu, C. Lhuillier, P. Sindzingre, P. Lecheminant, L. Pierre, *Eur. Phys. J. B* **2**, 501 (1998).
- 2 R. Moessner, J. T. Chalker, *Phys. Rev. Lett.* **80**, 2929 (1998).
- 3 B. Canals, C. Lacroix, *Phys. Rev. Lett.* **80**, 2933 (1998).
- 4 G. Misguich, C. Lhuillier, B. Bernu, C. W. Akhtamann, *Phys. Rev. B* **60**, 1064 (1999).
- 5 J. B. Fouet, M. Mambrini, P. Sindzingre, and C. Lhuillier, *Phys. Rev. B* **67**, 54411 (2003).
- 6 M. Johansson, K. W. Tomroos, F. Mila, P. Millet, *Chem. Mater.* **12**, 2853 (2000).
- 7 P. Lemmens, K.-Y. Choi, E. Kaul, Ch. Geibel, K. Becker, W. Brenig, R. Valent, C. Gros, M. Johansson, P. Millet and F. Mila, *Phys. Rev. Lett.* **87**, 227201 (2001).
- 8 W. Brenig, and K. W. Becker, *Phys. Rev. B* **64**, 214413 (2001).
- 9 K. Totsuka, and H. -J. Mikeska, *Phys. Rev. B* **66**, 54435 (2002).
- 10 R. Valent, T. Saha-Dasgupta, C. Gros, and H. Rosner, *Phys. Rev. B* **67**, 245110 (2003).
- 11 C. Gros, P. Lemmens, M. Voja, R. Valent, K.-Y. Choi, H. Kageyama, Z. Hiroi, N. V. Mushnikov, T. Goto, M. Johansson, and P. Millet, *Phys. Rev. B* **67**, 174405 (2003).
- 12 O. Zaharko, A. Daoud-Aladine, S. Streule, J. Mesot, P. J. Brown, and H. Berger, *Phys. Rev. Lett.* **93**, 217206 (2004).
- 13 M. Mambrini, J. Tribes, F. Mila, *Phys. Rev. B* **59**, 13806 (1999).
- 14 I. Bose, A. Tribedi, *Phys. Rev. A* **72**, 22314 (2005).
- 15 M. E. Lines, A. P. Ginsberg, R. L. Martin, R. C. Sherwood, *J. Chem. Phys.* **57**, 1 (1972).
- 16 D. H. Jones, *J. Chem. Phys.* **79**, 3877 (1983).
- 17 A. B. Blake, *J. Chem. Soc. Dalton Trans.* **1**, 2039 (1997).
- 18 L. F. Chibotaru, *Koord. Khim. iya* **15**, 634 (1989).
- 19 E. Buluggiu, *J. Chem. Phys.* **84**, 1243 (1986).
- 20 T. D. Black, R. S. Rubins, D. K. De, R. C. Dickinson, W. A. Baker Jr., *J. Chem. Phys.* **80**, 4620 (1984).
- 21 R. C. Dickinson, W. A. Baker, T. D. Black, R. S. Rubins, *J. Chem. Phys.* **79**, 2609 (1983).
- 22 V. Z. Polinger, L. F. Chibotaru, I. B. Bersuker, *Molecular Physics* **52**, 1271 (1984).
- 23 V. Z. Polinger, L. F. Chibotaru, I. B. Bersuker, *Phys. Stat. Sol. B* **129**, 615 (1985).
- 24 E. A. Goreschnik, V. V. Olijnyk, *Zhurnal Neorganicheskoi Khimii* **41**, 206 (1996).
- 25 J. P. Perdew, K. Burke and M. Ernzerhof, *Phys. Rev. Lett.* **77**, 3865 (1996).
- 26 P. Blaha, K. Schwarz, G. K. H. Madsen, D. Kvasnicka and J. Luitz *WIEN2k, An augmented Plane Wave + Local Orbitals Program for Calculating Crystal Properties* ed. K. Schwarz (Wien, Austria: Techn. University) ISBN 3-9501031-1-2.
- 27 G. Kresse and J. Furthmüller, *Phys. Rev. B* **54**, 11169 (1996).
- 28 G. Kresse and J. Hafner, *Phys. Rev. B* **47**, 558 (1993).
- 29 K. Parlinski in *Neutrons and Numerical Methods N<sub>2</sub>M*, eds. M. R. Johnson, G. Kearley and H. G. Buttner, *Amer. Inst. Phys., Conference Proceedings* **476**, p. 121 (1999).
- 30 T. Rog, K. Murzyn, K. Hinsen and G. Keller, *J. Comp. Chem.* **24**, 657 (2003).
- 31 Y. Filinchuk, D. Chernyshov, O. Zaharko in preparation.
- 32 V. I. Anisimov, J. Zaanen, O. K. Andersen, *Phys. Rev. B* **44**, 943 (1991).
- 33 The strength of the F coupling and number of F/AF couplings is arbitrary. Susceptibility data are not sufficient to establish the unique model.
- 34 We observe dramatic diminishing of the quality of crystals while cooling though  $T_c$  in a neutron single crystal diffraction experiment (unpublished). The Bragg peaks split by several degrees with fast cooling and broaden with slow cooling.
- 35 This statement can be extended to 5 K according to our single crystal neutron diffraction experiment.
- 36 S. Millet, M. Souhassou, C. Lecomte, *Acta Cryst. A* **60**, 455 (2004).
- 37 M. A. Abersold, B. Gillon, O. Plantevin, L. Pardi, O. Kahn, P. Bergerat, I. von Seggern, F. Tuczek, L. Ohlström, A. Grand, E. Lelièvre-Berna, *J. Am. Chem. Soc.* **120**, 5238 (1998).

FIG. 16: (Color online) Vibrational density of states for each atom type (top). The vertical, dashed line highlights pronounced minima at 5 meV in all partial DOS, except the oxygen vDOS, and the existence of lower frequency modes. Examples of these for deuterium, carbon and copper, are shown separately (down).

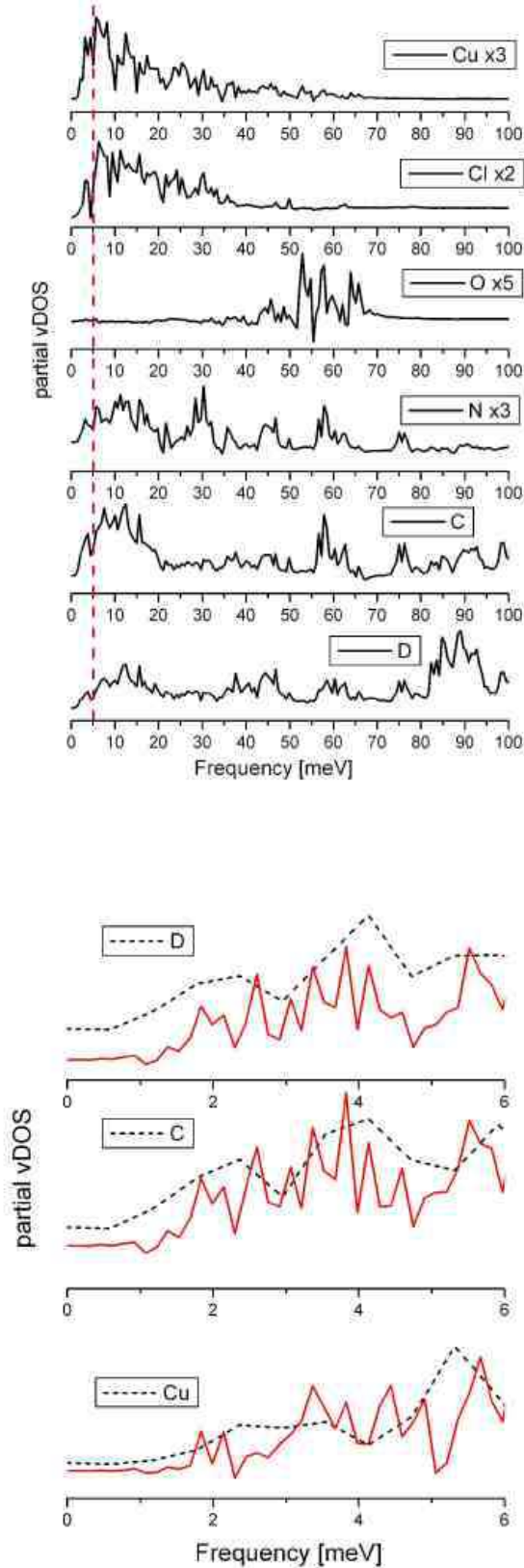


FIG. 17: Two-atom (bond) and four-atom (twist angle) correlations as a function of frequency from the MD calculation.

